Journal of Infrastructure Intelligence and Resilience 4 (2025) 100171

Contents lists available at ScienceDirect

Journal of Infrastructure Intelligence and Resilience

journal homepage: www.journals.elsevier.com/journal-of-infrastructure-intelligence-and-resilience

Data normalization for the continuous monitoring of a steel truss bridge: A case study from the Italian railway line

Antonio Argentino, Luca Radicioni, Francesco Morgan Bono, Lorenzo Bernardini *, Lorenzo Benedetti, Gabriele Cazzulani, Claudio Somaschini, Marco Belloli

Department of Mechanical Engineering, Politecnico di Milano, Via G. La Masa 1, Milano, 20156, Italy

ARTICLE INFO

Keywords:
Structural health monitoring
Railway bridge
Data normalization
Temperature treatment
Steel truss bridge

ABSTRACT

Structural health monitoring is recognized as a powerful tool to assist bridge management. Continuous long-term monitoring of bridge structures presents several challenges, including the need for effective system design, robust sensors deployment, efficient data management, and comprehensive data analysis and interpretation. In the field of operational modal analysis, automatic tracking of bridge frequencies over time has been shown to be significantly influenced by temperature fluctuations. This effect is also observed in low-frequency sampled signals. To address these issues, the authors present a double-step procedure to effectively mitigate the influence of temperature on the estimated modal parameters and raw signals from displacement, strain and rotation transducers. The procedure is based on multiple linear regression, taking the measured temperatures as inputs, followed by low-pass filtering operations applied to the residuals through moving averages, leading to the creation of minimum detectable anomaly curves. The latter allow to establish quantitative relationships between filtering window lengths and detectable damage thresholds at specified confidence levels. The case study involves a railway steel truss bridge, where more than a year of data was collected through a permanent monitoring system. The monitoring layout includes a variety of sensors deployed to measure the structural response, as well as environmental and operational variables. A 15-month dataset demonstrates how temperature compensation effectively reduces signal variability, which is crucial for enhancing early-stage anomalies detection.

1. Introduction

Given the concerning conditions of bridges and viaducts worldwide (Aflatooni et al., 2014; Lin et al., 2014; Dinas et al., 2017), structural health monitoring (SHM) has received increasing attention from both the academic community and industrial players (Gordan et al., 2022; Limongelli, 2019). SHM is being used as a complementary tool to visual inspections to address their potential limitations (Iacovino et al., 2022). SHM involves observing and analysing a system over time using sampled response measurements to investigate changes in the material and geometric properties of the structure. This practice serves multiple purposes, including enriching knowledge about the bridge (Vardanega et al., 2022), optimizing operations and maintenance (O&M) (Orcesi and Frangopol, 2011), and supporting emergency management in the case of extreme events (Giordano and Limongelli, 2022). Compared to visual inspections, SHM has the advantage of providing quantitative and potentially real-time data, enabling objective and timely evaluation of structural conditions. However, it presents challenges, primarily related to the structural complexity of bridges and the variety of phenomena they are subjected to.

From a broader perspective, this complexity hinders the achievement of the standardization needed for the rapid and widespread adoption of SHM across the network (Limongelli et al., 2022). On the other hand, when focusing on an individual bridge, the presence of multiple factors affecting the structural response complicates the effective utilization of acquired data for extracting meaningful information. As shown in related literature (Cross et al., 2013; Keshmiry et al., 2023), it is well known that environmental and operational variables (EOVs) strongly influence the signals measured by long-term monitoring systems (Mousavi and Gandomi, 2021).

Therefore, as suggested by several studies (Magalhães et al., 2012; Borlenghi et al., 2024; Reynders et al., 2014; Langone et al., 2017), including the present one, their compensation is crucial. Since the primary purpose of a health monitoring system is to recognize anomalies, damage identification can be significantly enhanced by purging environmental and operational variables (EOVs), thereby reducing signal

* Corresponding author.
E-mail address: lorenzo.bernardini@polimi.it (L. Bernardini).

https://doi.org/10.1016/j.iintel.2025.100171
Received 13 June 2025; Received in revised form 6 August 2025; Accepted 31 August 2025
Available online 15 September 2025
2772-9915/© 2025 The Authors. Published by Elsevier Ltd on behalf of Zhejiang University and Zhejiang University Press Co., Ltd. This is an open access article under the CC BY-NC-ND license (http://creativecommons.org/licenses/by-nc-nd/4.0/).

variance (Benedetti et al., 2023). The best practice in the literature addresses temperature – the main factor affecting measurement variability – through supervised learning techniques (Xia et al., 2012; Caspani et al., 2022). However, when EOVs are unmeasured, unsupervised learning approaches are commonly suggested. Among these, principal component analysis (PCA) stands out as a powerful tool to reduce variability from unknown sources (Comanducci et al., 2016; Khoa et al., 2014).

PCA allows for the identification of a coordinate system whose principal components (PCs) are uncorrelated (orthogonal) and hierarchically arranged so that the first principal components retain most of the dataset variance (Brunton and Kutz, 2019; Giordano et al., 2022; Wang et al., 2022). However, the use of PCA poses some concerns. First, by removing the contribution of the main PCs, it becomes impossible to identify anomalies that can be expressed as a linear combination of those PCs, meaning that even if damages occur in the structure, they cannot be observed. Second, there is no general agreement in the literature on how many PCs must be removed to achieve optimal system performance.

Conversely, this study proposes a novel, physically interpretable two-step methodology for data normalization that explicitly addresses the trade-off between damage detectability and damage evolution dynamics. The core contributions are:

1. A hybrid approach combining multiple linear regression (for measured temperature compensation) with adaptive moving average filtering (for residual noise reduction), enhancing sensitivity to structural changes.
2. The presentation of minimum detectable anomaly (MDA) curves (Radicioni et al., 2023), which quantitatively link filtering window lengths to detectable damage thresholds under specified confidence levels. These curves enable practitioners to: (i) estimate detection time for damage of known severity, and (ii) design control charts tailored to damage evolution rates (slow vs. rapid).
3. Explicit reconciliation of the delay introduced by filtering with damage evolution velocity—a critical aspect often overlooked in EOV compensation schemes. This framework dynamically adapts sensitivity based on the expected damage scenario (Table 2).

Unlike PCA-based methods that risk masking damage-related features (Brunton and Kutz, 2019; Giordano et al., 2022), the procedure presented in this work retains the physical interpretability of residuals while systematically reducing uncertainty. Furthermore, the MDA curves provide a formalized strategy for damage detection under varying operational conditions, directly overcoming the lack of a general rule for determining how many PCs should be removed. The used approach encompasses all the phases outlined in the literature for data normalization: measurement of environmental and operational variables (EOVs), low-frequency analysis, dynamic analysis, and finally, compensation of the environmental effects on the obtained results.

The remaining paper outline is organized as follows. Section 2 is devoted to describing the bridge and the design of its permanent monitoring system. Section 3 outlines the methodologies employed in data analysis, specifically addressing the automated operational modal analysis (AOMA) performed through the covariance-driven stochastic subspace identification (SSI-COV) algorithm, and the technique used to mitigate the temperature effect on static signals and modal parameters. Section 4 reports results about SSI-COV-based operational modal analysis. Then, the performance of the temperature mitigation algorithm is critically discussed. Finally, conclusions are drawn in Section 5, by presenting the main achievements of the work and possible future outlooks.

2. Case study bridge and permanent monitoring system

The subject of this paper is the Warren truss railroad bridge depicted in Fig. 1. Constructed in 1946, this bridge is inserted in the Italian railway network. The bridge comprises two twin structures, one for each travel direction, supported by the same pier and abutments. These structures consist of two spans of different lengths: the longer one crosses riverbed while the shorter one lies above the floodplain.

In the framework of a project conducted with the infrastructure manager, the upstream bridge was equipped with a permanent monitoring system, schematically summarized in Fig. 2, put into service in July 2022. The bridge hosts the following sensing devices, according to the scheme in Fig. 2:

Velocimeters These instruments allow for studying the vibrations of the bridge and the pier. Positioned to estimate the bridge's dynamic properties, these transducers allow to distinguish between lateral, bending, and torsional vibrations. The pier-mounted velocimeter, on the other hand, enables seismic-type monitoring.

Tiltmeters Installed at the four corners of each monitored span, the tiltmeters allow to qualitatively reconstruct bridge shape over time, identifying possible weakening of the span structure. These are mono-axial sensors, measuring the rotation around the Y axis. Additionally, a bi-axial sensor is installed on the pier, specifically monitoring sudden damage related to local scour around the pier. This sensor measures rotations around both the X and Y axes.

Linear variable displacement transducers (LVDTs) These instruments are displacement sensors, allowing the continuous monitoring of bridge elongation over time. This helps in detecting potential issues with the mobile supports, bridge deck or asymmetries in thermal expansion behaviour.

Local micro-strain gauges Only the most stressed bridge members – external diagonals and lower chords – are subject to strain measurement, to maintain cost-effectiveness and scalability in the monitoring system. These elements are equipped with micro-strain gauges to measure the axial forces acting on them.

Weigh-in-motion stations A second strain gauge system, mounted along one rail, enables a weigh-in-motion (WIM) procedure. These strain gauges feature a full-bridge configuration and are positioned on both sides of the rail at a 45 ° angle to the neutral axis. They assess shear strain, compensating for the influence of temperature, axial and bending actions. The WIM system consists of two measurement spans placed 18 m apart, each made of a pair of measurement sections, and enables the recognition of train speed and acceleration, axle number, load, and spacing.

Resistance temperature detectors (RTDs) Temperature monitoring occurs in two ways: air temperature is measured by a nearby weather station (few meters from bridge entrance), and four RTDs, positioned at the entrance of the longest span, directly measure the structure's temperature. Placed at the four corners of the span's entrance portal, the RTDs offer a representative estimate of structure temperature distribution and a more accurate assessment of the structure's average temperature when needed. Given the similarity of the two spans and the fact that both are exposed to the same sunlight conditions, only span A has been instrumented. Nevertheless, the average temperature values of the structure will be used to characterize the behaviour of span B as well, for the reasons mentioned earlier.

(a) (b)

Fig. 1. Warren truss bridge under analysis. (a) Frontal view. (b) Side view.

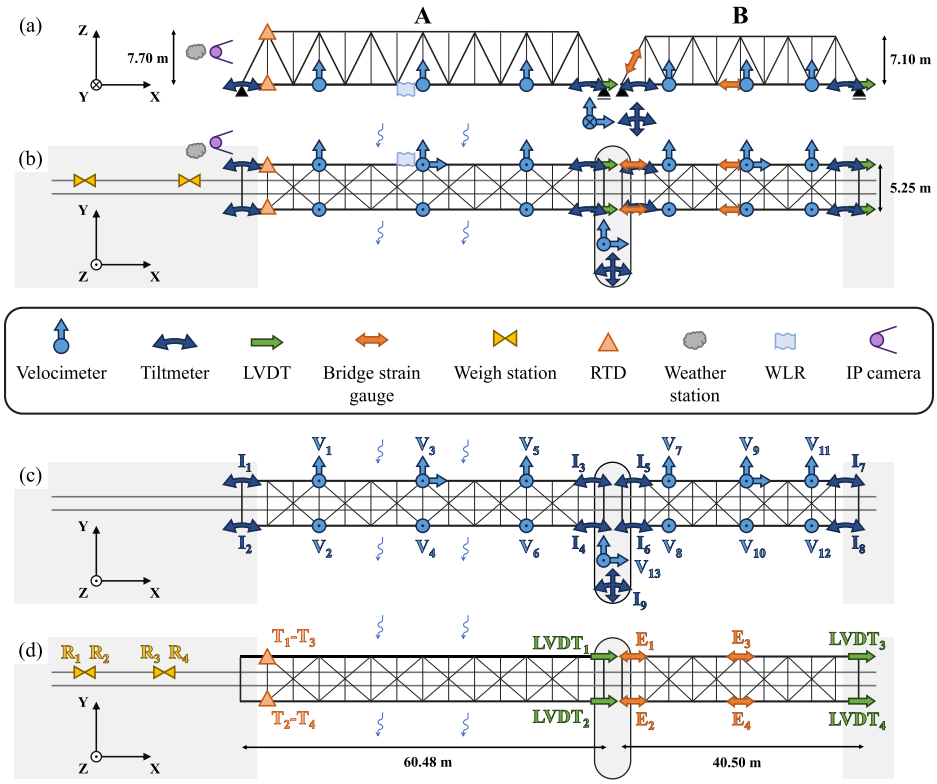

Fig. 2. Sensors placement along spans A and B. (a) Side view. (b) Top view. (c)-(d) Representation of the various sensors with their respective IDs (Top view). Main geometrical features of the bridge are reported as well.

Weather station The weather station also measures other meteorological parameters of potential interest: air pressure, temperature and humidity, temperature and humidity within the station's housing, wind direction and speed, rainfall, and solar radiation.

Water level radar (WLR) A WLR sensor is centrally mounted in the streambed span to monitor the water level, which is relevant in the event of sudden floods.

IP camera Lastly, the bridge is equipped with an IP camera capable of transmitting real-time photos or videos of the pier, facilitating the monitoring of debris accumulation against it.

From the item listed above, it is clear that the adopted sensor mesh allows for the continuous monitoring of bridge response due to operational and environmental inputs in different frequency ranges of interest.

A unique acquisition and datalogging system, installed close to the bridge, manages all the sensing devices. The datalogger is based on National Instruments cRIO modular system, equipped with proper A/D modules and enabled to RS232 communication with the weather station, TCP/IP communication with the IP camera and internet communication through a router. This system stores data locally for buffering purposes and automatically and continuously sends them to the users, who can remotely change, at any moment, the acquisition properties associated with each measuring channel. The datalogging systems acquires three different file typologies for different purposes:

Continuous logging To register the static behaviour of the bridge over time, data are acquired and logged at low frequency (i.e., sampling frequency of 1 Hz) . The list of channels to be saved can be programmed by the user and typically involves all the sensors related to long-term monitoring of the static behaviour of the bridge (tiltmeters, strain gauges, displacement sensors), as well as the environmental sensors. Also dynamic sensors can be continuously acquired to perform continuous operational modal analysis OMA, provided that the bridge vibrations under natural excitation are strong enough compared to the sensitivity of the sensors. The installed system acquires data from velocimeters at 128 Hz in continuous logging.

Triggered logging This logging refers to event-triggered conditions, where the trigger is fired when one or more sensors reach a certain value. Also the parameters of this acquisition type can be set similarly to the continuous logging (plus two options for

Table 1
Sensors IDs, typology, model and sampling frequencies, in continuous and triggered logging (i.e., c.l. and t.l. respectively). Please notice that sensors' IDs are referred to Fig. 2.

Sensor ID	Sensor Type	Sensor model	f_{samp} c.l. [Hz]	f_{samp} t.l. [Hz]
V_{1-13}	Velocimeters	Sara SS45	128	256
I_{1-8}	Tiltmeters (servo)	SMIC-L-3	1	64
I_9	Tiltmeter (MEMS)	NS-5/DMG2-I	1	/
R_{1-4}	Strain gauges (WIM)	HBK 1-XY41-6/120	/	2048
T_{1-4}	RTDs	PT100	1	/
$LVDT_{1-4}$	LVDTs	ISDG50-K2–2442	1	64
E_{1-4}	Strain gauges	HBK 1-XY71-6/120	1	64
WLR	Water level radar	VEGAPULS C23	1	/
IPC	IP camera	Basler BIP2	0.00028	/
WS	Weather station	Vantage Pro2	1	/

pre and post trigger) and, in this specific application, this is used to store higher frequency (sampling frequency equal to 256 Hz) data in presence of events such as train passages (on the bridge under monitoring and on the twin one), floods or earthquakes. The data coming from train passages are used specifically for modal identification (isolating bridge free decays after train transits) and to identify the characteristics of the convoys.

Pictures Screenshots from the IP camera are saved regularly with a programmable frequency to assess debris accumulation against the pier. In case of flood, this frequency can be increased to monitor debris arrival more promptly.

For each installed device, information regarding sensor typology and model are collected in Table 1, as well as the sampling frequencies in continuous and triggered logging respectively. The acquisition frequencies were selected based on the physical phenomenon to be captured and the dynamics involved. Specifically, sampling frequencies of 1 Hz were chosen to capture the static behaviour of the structure (deck or pier). Velocimeters operate at the highest sampling frequency in continuous logging mode, with 128 Hz rate ensuring proper identification of the main modes of the bridge. In triggered mode, the acquisition frequencies are higher, regardless the nature of the sensor: this choice ensures the capture of higher-frequency harmonics induced by train passages over the structure. Still within the triggered acquisition mode, a sampling frequency of 2048 Hz was selected for the WIM system to allow for accurate estimation of the speed, weight, and geometric spacing of railway loads crossing the bridge.

3. Methodology

This section presents the methodology used to estimate natural frequencies and mode shapes. Following this, a two-step approach is established to compensate for temperature-induced variations.

3.1. Covariance-driven SSI algorithm for automatic operational modal analysis

Covariance-driven stochastic subspace identification (SSI-COV) is a well-known time-domain methodology for modal identification, which belongs to the family of subspace identification methods (Deraemaeker and Worden, 2012). In this work, the accelerations obtained from measured velocity histories (see Fig. 2) are exploited to extract bridge modal parameters through the application of a stochastic state-space model, defined as follows:

$$\begin{cases} \{x_{k+1}\} = [A]\{x_k\} + \{w_k\} \\ \{y_k\} = [C]\{x_k\} + \{v_k\} \end{cases} \tag{1}$$

where x_k represents the discrete-time state vector at the k-th time instant, while [A] is the discrete state matrix; y_k is the measured output and [C] is the output discrete matrix. Moreover, w_k and v_k are respectively referred to as model inaccuracies and measurement noise due to sensors (Magalhães et al., 2009).

Once [A] and [C] matrices are estimated through acceleration time histories, it is possible to compute bridge modal parameters, starting from the eigenvalue decomposition of the state matrix (Ewins, 2009). Unlike most works applying SSI-COV to the bridge's ambient vibration response, in this study, the algorithm processes structural free decays consequent to train passages, similarly to Salehi and Erduran (2022). The free decays are automatically isolated by combining a fast and a slow moving-time windowing operations, as illustrated in Argentino et al. (2023).

The SSI-COV algorithm needs two key parameters in input to perform modal identification properly: the number of correlation points and the system order. The former is used for covariance computation, which is related to the dimension of the Toeplitz covariance matrices (Tomassini et al., 2023). Given its strong influence on the quality of the resulting stabilization diagram, this parameter must be finely tuned by running some preliminary tests, as reported in Magalhães et al. (2009). The order of the system is associated with the number of degrees of freedom required by the model to properly approximate the measured dynamic behaviour of the actual system. This value is not known a priori when dealing with real structures (e.g., civil structures): therefore, a guess must be done, given the frequency range of interest.

Assuming a high-order model leads to spurious modes (also called noise modes) that are needed to model the noise present in the measurements. These modes have low or none physical meaning; therefore, it is crucial to separate physical and spurious modes and the so-called stabilization diagram accomplishes this task. In particular, the evaluation of stable and spurious poles is based on three criteria of stability, respectively set on frequency, damping ratio and mode shape (through MAC computation), as reported in the following set of equations (Kvåle et al., 2017):

$$\frac{\left|f_{p+k+1} - f_{p+k}\right|}{f_{p+k}} < 1\% \tag{2}$$

$$\frac{\left|\xi_{p+k+1} - \xi_{p+k}\right|}{\xi_{p+k}} < 2\% \tag{3}$$

$$1 - MAC\left(\{\phi_{p+k+1}\}\{\phi_{p+k}\}\right) < 2\% \tag{4}$$

where k value ranges from 0 to 3 and f_p, ξ_p and $\{\phi_p\}$ are respectively the frequency, damping ratio and mode shape associated with a pole of the p-th order system. In this way, a pole is considered stable if the conditions above are met for four successive system order poles. In order to automatize the procedure for daily extraction of modal parameters, a clustering algorithm based on (Civera et al., 2023) is implemented. Therefore, in a first stage, it is possible to remove noise modes and, subsequently, to clusterise the stable poles related to the different mode shapes.

To select the number of correlation points, i, a two-step approach, based on related literature (e.g., Zini et al. (2022)), was followed. First, a baseline was established using the formula $i \geq \frac{f_s}{2f_0}$, where f_s is the

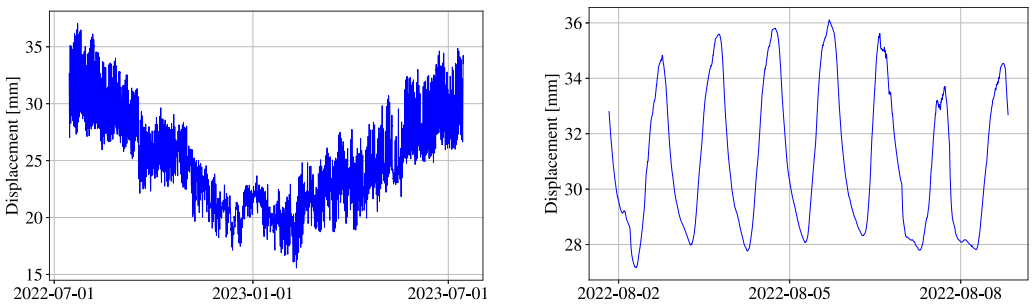

Fig. 3. Time behaviour of a displacement transducer ($LVDT_3$, see Fig. 2). (a): throughout a year. (b) throughout a week (b). The signal is acquired at 1 Hz (refer to Table 1).

sampling frequency and f_0 is the bridge's first natural frequency. The f_0 value was determined by applying a manual Frequency Domain Decomposition (FDD) to the initial data acquisitions. Subsequently, several values were tested for the parameter i, based on this initial calculation. Precisely, defined a base value as $m = \frac{f_s}{2f_0}$, a list of multiples $(2m, 3\ m, 4\ m, 5m)$ to be used was evaluated. The different results, in terms of stable poles, obtained with each i value, are then joined.

3.2. Normalization of environmental factors

Considering the signals acquired from LVDTs, tiltmeters and strain gauges, it is possible to notice that two components dominate the signals' trend: a daily periodicity and a seasonal trend, as shown in Fig. 3. These fluctuations are considered part of the structure's nominal behaviour as they were recorded during a period of normal operation. Instead, given that the OMA algorithm estimates one modal parameter value per day, only a seasonal trend can be observed for these.

Local temperature is widely considered the dominant factor driving this low-frequency behavior (Comanducci et al., 2016), a conclusion supported by the results in Section 4.2, where temperature is shown to have a clear influence on most measurements. To explain the behaviour of the bridge under thermal load induced by temperature variations, a possible approach could be the use of a model that considers the thermal expansion of the materials, as done in Nassar and Amleh (2023). However, this would involve the definition of a complex thermal model specific to this bridge, which is beyond the scope of this research project, oriented instead to a replicable approach of SHM. Other approaches rely on fitting data-driven models, whose performances exclusively depend on the selected training set. In fact, due to the presence of the exogenous inputs, Eq. (5) holds (Gianesini et al., 2021):

$$y = y_{\mathrm{T,ref}} + \Delta y_{\mathrm{T}} + \Delta y_{\mathrm{u}} + \Delta y_{\mathrm{n}} \tag{5}$$

where y represents the measured (or estimated) value for a feature, $y_{\mathrm{T,ref}}$ is the true value of the feature at a reference temperature, Δy_{T} is the contribution of temperature variations on the feature (as well as other measured exogenous factors), Δy_{u} the variation imputable to the exogenous not measured variable (such as disturbances or defects) and Δy_{n} the contribution due to measurement noise. Data normalization consists then in the reduction of the elements which mask the true reference value, hence Δy_{T}, Δy_{u} and Δy_{n}. In literature, the contribution due to measurable variables (such as Δy_{T} in Eq. (5)) is commonly modelled through supervised algorithms, whereas the contribution resulting from immeasurable variables (Δy_{u}) is addressed by unsupervised learning methods (Wang et al., 2022; Jiang et al., 2022; Bono et al., 2023; Mariani et al., 2024).

To train a learning model, it is essential to identify the period of the acquisition that corresponds to the baseline, during which the structure is reasonably assumed to be healthy. The method should then be capable of detecting any changes in the data compared to what is present in the baseline (Figueiredo et al., 2014). If the dataset can be represented by a data matrix, where n is the number of features and m is the number of time steps (Eq. (6)), defining the baseline involves identifying the index $t < m$ that corresponds to the undamaged structure. In this way, the baseline (or training set) for the algorithm can be established.

$$\mathbf{X} = \begin{bmatrix} \mathbf{x}_1 & \mathbf{x}_2 & \dots & \mathbf{x}_m \end{bmatrix} \tag{6}$$

Focusing on static regression models (supervised learning approach), the objective is to create a model for each feature, that takes in input the temperatures measured in different locations of the bridge to predict the feature values themselves, for every time snapshot. In fact, by estimating a function that takes as input the temperature vector $\mathbf{T}_i$ at the $i\text{-}th$ time snapshot and estimates the feature value (see Eq. (7)), it is possible to remove the influence of the environmental effect as shown in Eq. (8):

$$\hat{\mathbf{y}}_i = \hat{\mathbf{f}}(\mathbf{T}_i) \approx \Delta \mathbf{y}_{\mathrm{T},i} \tag{7}$$

$$\mathbf{e}_i = \mathbf{y}_i - \hat{\mathbf{y}}_i \approx \mathbf{y}_{\mathrm{T,ref},i} + \Delta \mathbf{y}_{\mathrm{u},i} + \Delta \mathbf{y}_{\mathrm{n},i} \tag{8}$$

where $\mathbf{e}_i$ is the residuals vector at the $i\text{-}th$ snapshot, hence the contribution to the features which is not imputable to temperature. In the present case, the regressor applied is a static multiple linear regression for each feature, in the form of:

$$\hat{\mathbf{y}}_i = \mathbf{A}^T \mathbf{T}_i + \mathbf{b} \tag{9}$$

where $\mathbf{A}$ is the matrix of weights and $\mathbf{b}$ the bias vector, both estimated by fitting the regressors onto the baseline with a least-square minimization approach, operated separately on each feature (Uyanık and Güler, 2013). One year of training set (or baseline) is most of the time sufficient to capture the entire seasonality that the structure experiences. As an example, Fig. 4 illustrates the time history regarding $LVDT_3$ sensor (plotted in blue) and the resulting residual after regression was applied (drawn in orange). As a result, main seasonal oscillations (low frequency ones) are totally removed by the static regression operation, while higher frequency variability is still present in the residuals. In fact, under the assumption that regression has been successfully applied, the residual $\mathbf{e}_i \approx \mathbf{y}_{\mathrm{T,ref},i} + \Delta \mathbf{y}_{\mathrm{u},i} + \Delta \mathbf{y}_{\mathrm{n},i}$ is mainly influenced by the unmeasured external effects and measurement noise only. Focusing now on the term $\Delta \mathbf{y}_{\mathrm{n},i}$ and assuming that the measurement noise acts as white noise (i.e, flat spectrum), the high-frequency contributions can be attenuated by applying a low-pass filtering operation. Compared to other low-pass filters, a *moving average* is easily understandable and can be immediately visualized. Empirically, it can be observed that the application of moving averages with longer averaging windows generates a signal whose distribution is characterized by a lower standard deviation. This is illustrated in Fig. 5, where an example of

Table 2
Anomaly evolution velocity versus damage extent. All possible scenarios.

		Anomaly evolution velocity	
		Slow	Fast
Anomaly extent	**Minimal variation**	A small damage whose evolution in time is particularly slow can be identified with an average window sufficiently long, with no safety concern.	If a small damage is happening, but the evolution is fast, it might not be detectable with a proper advance, because the available time window is insufficient.
	Sensible variation	A damage whose propagation in time is slow, but produces sensible variation in measurements, can be identified even with a small averaging window.	If a relevant variation due to damage is underway, whose evolution in time is fast, it might be detected in a useful time.

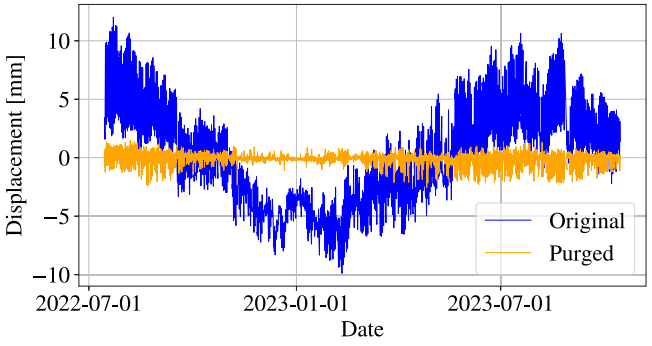

Fig. 4. Example of a feature (time series acquired by $LVDT_3$) before and after temperature purging, performed by multiple linear static regression. The original signal (minus the average value) is drawn in blue, while its residual is plotted in orange.

residuals averaged with windows of different sizes is represented in the time domain (Fig. 5(a)), whereas the associated best-fitting Gaussian distributions are displayed alongside (Fig. 5(b)). The idea behind the use of moving averages is to "shrink" the distributions up to a point where the effects of structural anomalies can be appreciated with a higher confidence interval.

By applying longer and longer moving average windows, and considering the standard deviation associated with each filtered signal obtained in such a way, it is possible to obtain the curves in Fig. 6, where for each window length, three confidence levels are considered. This curves have been called *minimum detectable anomaly* (MDA) curves, since they represent the minimal variations in the residuals that cannot be attributed to the normal behaviour of the structure.

In the example shown in Fig. 6, the confidence levels addressed are 90%, 95% and 99%, which corresponds to 1.65, 1.96 and 2.57 the standard deviation, respectively. Given a moving average window w_k, the three values for the residuals obtained ($r_{k,90}$, $r_{k,95}$ and $r_{k,99}$) represent the probability that a new observation extracted from the distribution falls into the interval considered. On the contrary, the observations that fall outside the interval can be interpreted as outliers, corresponding to potential anomaly condition for the structure. The drawback of using moving averages, as well as low-pass filtering in general, is that they introduce a certain delay (strictly proportional to the window length) between the availability of new measurements and the averaged value. This means that the shrinking of residual distributions comes at the cost of the delay to obtain a value which can be compared to those nominal distributions (i.e. Gaussian distributions extracted from the baseline period). This fact raises concerns related to the evolution velocity of an anomaly against the time necessary to detect it, as synthetically explained in Table 2. To conclude, applying moving averages may represent a good strategy to identify those damages whose evolution in time is longer than the window applied. For damages distinguished by rapid evolution, it appears necessary to use short windows or not use moving averages at all, accepting that those anomalies might be observed only when they reach significant amplitudes. Therefore, according to the authors, these considerations might be carefully addressed in the design and implementation of an SHM strategy based on this treatment of environmental factors.

4. Results

This section presents the results obtained by applying the previously described methodologies to the data collected during the monitoring period. First, the outputs from the covariance-driven stochastic subspace identification (SSI-COV) algorithm will be presented and critically discussed. Following that, the focus will be posed on addressing the effects of temperature on direct and indirect measurements (i.e., modal parameters).

4.1. Operational modal analysis

Through the procedure outlined in Section 3.1, it has been possible to estimate the modal parameters for both spans A and B (see Fig. 2) for the time period ranging from July 2022 to October 2023, for a total amount of 15 months of data. For span A, eight vibration modes were identified, comprising six lateral bending modes, one vertical bending mode, and one torsional mode. Conversely, for span B, a total of seven vibration modes were identified, including five lateral bending modes, one vertical bending mode, and one torsional mode.

A nomenclature convention has been adopted, starting with a letter that stands for the mode type (Lateral, Vertical, or Torsional), followed by a number indicating the mode order, and finally, a letter to distinguish different variants of the same mode order. All the identified mode shapes for span A are illustrated in Fig. 7. In this figure – referred to span A – in addition to the median mode shapes over the monitoring period, a variability band is represented, ranging from the 10th to 90th percentile of the experimental population, containing the modes estimated each day. Similar modal shapes, not reported here for the sake of brevity, are derived for span B.

The natural frequencies show a strong linear correlation with temperature for the majority of modes, in agreement with related literature (Xia et al., 2012; Zhou and Yi, 2014; Han et al., 2021). Fig. 8 depicts all daily values of natural frequency (as a function of time and temperature) and damping ratio, in relation to temperature, for three modes of primary interest in span A. The modes were chosen to exhibit varying degrees of frequency and damping correlation with temperature. The modes depicted in Fig. 9 were selected using the same rationale, for span B. The only mode displaying a significantly lower correlation is L2 A, whose frequency appears to be independent of temperature. This observation is valid for both spans A and B (see Figs. 8 and 9).

As shown in both figures, the (mostly) linear correlation between temperature and natural frequency could be negative, neutral, or even positive. When dealing with damping ratios, the observed correlation with temperature is generally low, indicating that this parameter is not significantly influenced by temperature. However, this is not true for mode L3 A in span A, which exhibits a moderate level of temperature-damping correlation (Fig. 8). Furthermore, for modes V1 and L1B in

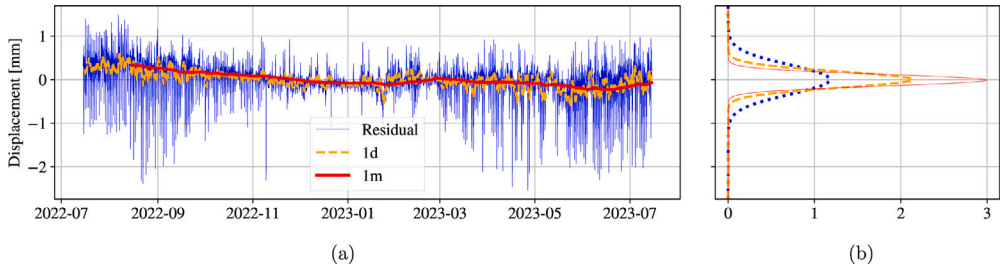

Fig. 5. Residuals for $LVDT_3$ with different moving averages (a) and associated Gaussian distributions (b). Please notice that 1d and 1 m refers to a one-day and a one-month windowing interval respectively.

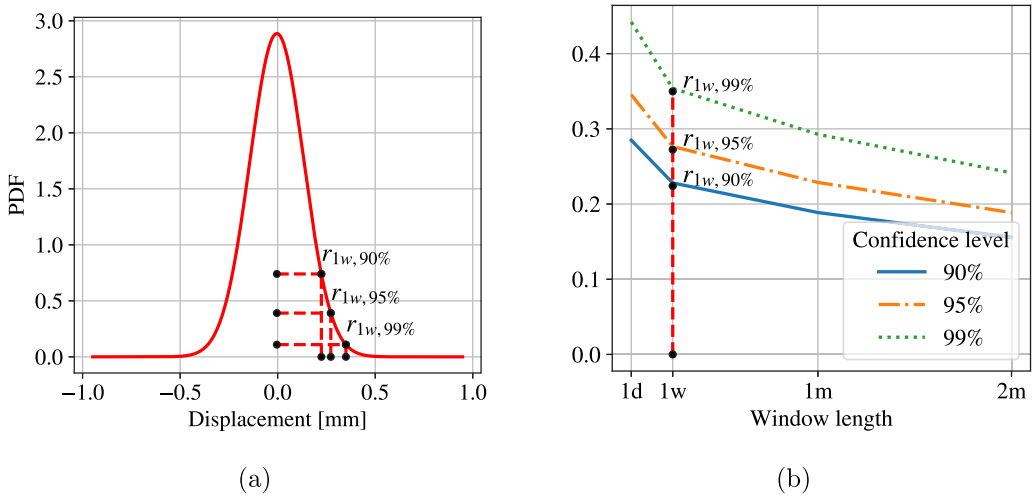

Fig. 6. Gaussian distribution associated to sensor $LVDT_3$ averaged with a 1-week-long window (a) and relative minimum detectable anomaly curve (b). Please notice that 1d and 1w refers to a one-day and a one-week windowing interval respectively. Moreover, 1 m and 2 m identifies 1-month-long and 2-month-long intervals.

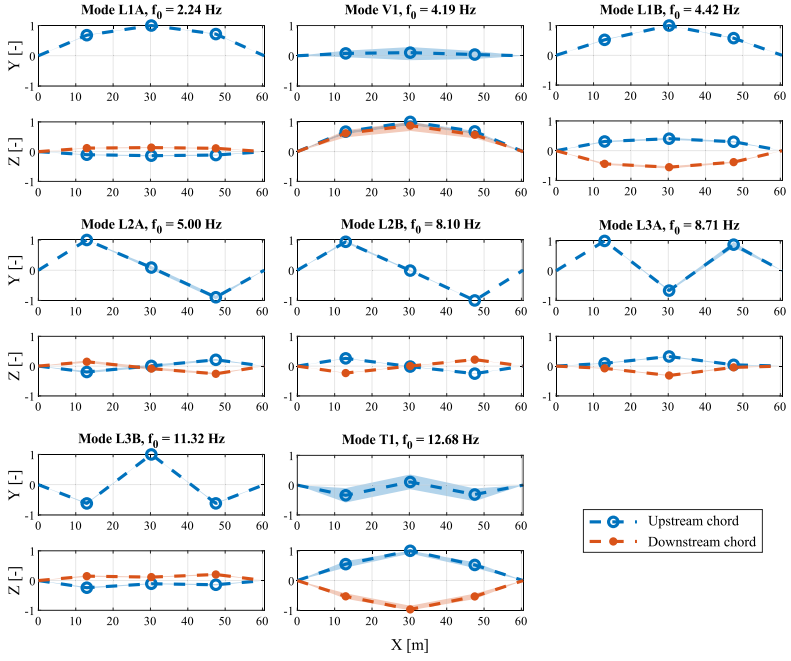

Fig. 7. Overview of the estimated modal shapes for span A, also highlighting a variability band between the 10th and 90th percentiles of the experimental population.

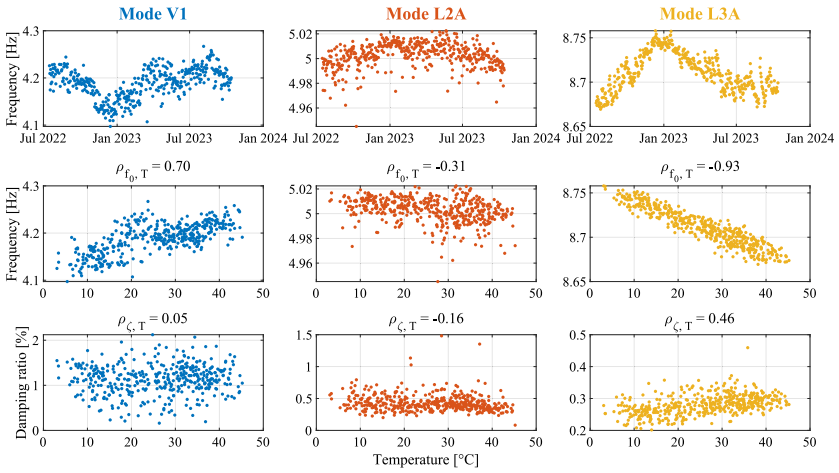

Fig. 8. Span A – Three relevant natural frequencies plotted over time and as functions of mean temperature, along with their corresponding damping ratios plotted with respect to temperature.

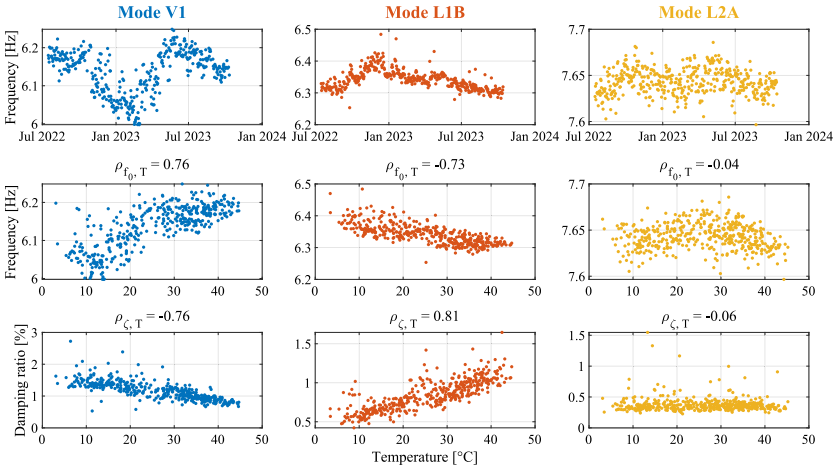

Fig. 9. Span B – Three relevant natural frequencies plotted over time and as functions of mean temperature, along with their corresponding damping ratios plotted with respect to temperature.

span B, the estimated damping ratios show a high level of correlation with temperature, notably opposite in sign (Fig. 9). Then, the modal assurance criterion (MAC) (Pastor et al., 2012) was employed to evaluate the stability and evolution of the mode shapes over time. For each mode shape, the MAC is calculated by comparing its daily estimate with a baseline mode shape. This baseline is selected from a 30-day initial monitoring period during which mode shapes are estimated daily. The MAC values resulting from pairwise comparisons of all daily estimates form a 30 × 30 matrix (being the monitored period 30-day long). The baseline mode shape is chosen as the one corresponding to the matrix row with the highest sum of its elements. In other words, the mode shape used as a reference is the one most similar (in terms of MAC value) to those estimated over the other 29 days. This selection process is repeated for each frequency of interest. Consistent with previous research (Xia et al., 2012; Zhou and Yi, 2014; Han et al., 2021), MAC does not correlate with temperature for any of the modes. For this reason, a representation of the MAC dispersion throughout the year for all identified modes was chosen, depicted through a set of boxplots in Fig. 10. First-order lateral modes exhibit less dispersion than higher-order modes. Additionally, modes with a predominant vertical component feature a sensibly greater dispersion than lateral modes.

4.2. Normalization of environmental factors

Table 3 displays the results obtained after applying the temperature treatment (first step of data normalization), for the training year. This process consists in the computation of residuals through multilinear regression. Due to the high number of sensors and modal parameters available, for the sake of conciseness, only some features are here considered: three tiltmeters, three LVDTs, three bridge strain gauges, and three natural frequencies related to span A and three for span B, together with the associated damping ratios. The environmental factors considered for the sensors are the four temperatures measured by RTDs. For the natural frequencies and damping ratios, having just one measurement per day, the regression considers the average temperature value corresponding to the isolated free-decays exploited by the SSI-COV algorithm to extract bridge modal parameters.

The regression model employed is a static linear one (see Eq. (9)), as other regression models did not yield better results on this dataset (Radicioni et al., 2023). The training period for the regressors is a complete year, from 15th July 2022 to 14th July 2023, while the test period ranges from 15th July 2023 to 15th October 2023. The metric chosen to evaluate the performance of the regression model in purging temperature influence is the standard deviation (s), that

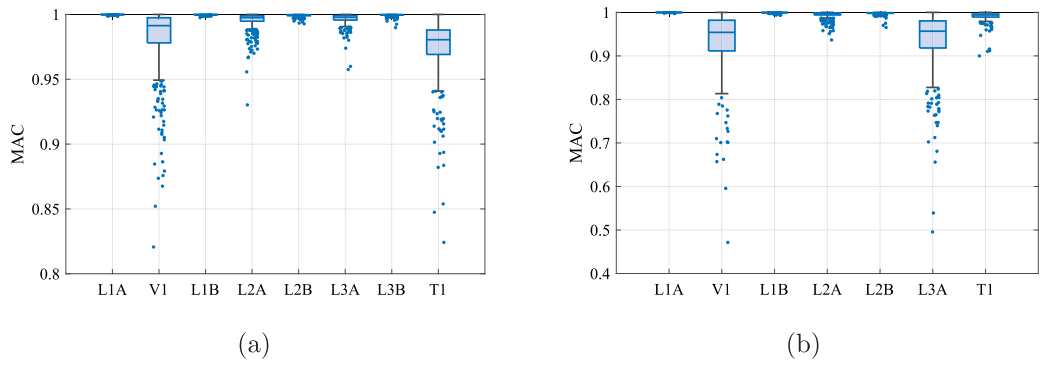

Fig. 10. Boxplot representation of the populations of MAC values for the estimated mode shapes. (a) Span A. (b) Span B.

Table 3
Standard deviations in the original measurements and after the treatment of the environmental factors, for the training dataset. ζ is the damping ratio, f the natural frequency. For sensors' IDs, please refer to Fig. 2.

	Original s (complete)	Purged s (complete)	% Reduction (complete)	Original s (week)	Purged s (week)	% Reduction (week)
$\mathbf{I_3}$ [°]	$4.58 \cdot 10^{-2}$	$3.19 \cdot 10^{-2}$	−30.3	$1.61 \cdot 10^{-2}$	$1.03 \cdot 10^{-2}$	−35.9
$\mathbf{I_4}$ [°]	$3.62 \cdot 10^{-2}$	$3.41 \cdot 10^{-2}$	−5.79	$1.50 \cdot 10^{-2}$	$1.41 \cdot 10^{-2}$	−5.99
$\mathbf{I_{9X}}$ [°]	$2.32 \cdot 10^{-2}$	$9.90 \cdot 10^{-3}$	−57.4	$3.70 \cdot 10^{-3}$	$8.00 \cdot 10^{-3}$	115
$\mathbf{LVDT_2}$ [mm]	4.29	$5.56 \cdot 10^{-1}$	−87.0	1.77	$3.32 \cdot 10^{-1}$	−81.3
$\mathbf{LVDT_3}$ [mm]	4.14	$3.39 \cdot 10^{-1}$	−91.8	1.71	$2.79 \cdot 10^{-1}$	−83.7
$\mathbf{LVDT_4}$ [mm]	4.03	$3.54 \cdot 10^{-1}$	−91.2	1.60	$2.71 \cdot 10^{-1}$	−83.1
$\mathbf{E_2}$ [$\mu\varepsilon$]	5.03	3.42	−32.1	4.49	2.80	−37.7
$\mathbf{E_2}$ [$\mu\varepsilon$]	5.97	2.62	−56.1	4.24	2.17	−48.8
$\mathbf{E_3}$ [$\mu\varepsilon$]	8.55	2.44	−71.4	5.93	1.95	−67.2
Span A: f_{V1} [Hz]	$3.16 \cdot 10^{-2}$	$2.33 \cdot 10^{-2}$	−26.0	$1.70 \cdot 10^{-2}$	$1.73 \cdot 10^{-2}$	1.50
Span A: f_{L2A} [Hz]	$1.03 \cdot 10^{-2}$	$9.80 \cdot 10^{-3}$	−5.61	$7.60 \cdot 10^{-3}$	$8.00 \cdot 10^{-3}$	4.94
Span A: f_{L3A} [Hz]	$2.14 \cdot 10^{-2}$	$7.60 \cdot 10^{-3}$	−64.5	$6.30 \cdot 10^{-3}$	$5.80 \cdot 10^{-3}$	−8.75
Span A: ζ_{V1} [-]	$3.40 \cdot 10^{-3}$	$3.40 \cdot 10^{-3}$	−0.45	$3.00 \cdot 10^{-3}$	$3.00 \cdot 10^{-3}$	0.55
Span A: ζ_{L2A} [-]	$1.30 \cdot 10^{-3}$	$1.20 \cdot 10^{-3}$	−8.84	$1.10 \cdot 10^{-3}$	$1.10 \cdot 10^{-3}$	−5.22
Span A: ζ_{L3A} [-]	$3.00 \cdot 10^{-4}$	$3.00 \cdot 10^{-4}$	−12.1	$2.00 \cdot 10^{-4}$	$2.00 \cdot 10^{-4}$	0.65
Span B: f_{V1} [Hz]	$6.11 \cdot 10^{-2}$	$3.89 \cdot 10^{-2}$	−36.4	$2.76 \cdot 10^{-2}$	$2.40 \cdot 10^{-2}$	−13.3
Span B: F_{L1B} [Hz]	$2.94 \cdot 10^{-2}$	$2.13 \cdot 10^{-2}$	−27.6	$1.37 \cdot 10^{-2}$	$1.41 \cdot 10^{-2}$	2.44
Span B: f_{L2A} [Hz]	$1.42 \cdot 10^{-2}$	$1.42 \cdot 10^{-2}$	0.06	$1.17 \cdot 10^{-2}$	$1.14 \cdot 10^{-2}$	−3.14
Span B: ζ_{V1} [-]	$3.00 \cdot 10^{-3}$	$2.00 \cdot 10^{-3}$	−31.5	$1.80 \cdot 10^{-3}$	$1.60 \cdot 10^{-3}$	−9.32
Span B: ζ_{L1B} [-]	$2.10 \cdot 10^{-3}$	$1.20 \cdot 10^{-3}$	−44.6	$9.00 \cdot 10^{-4}$	$8.00 \cdot 10^{-4}$	−15.7
Span B: ζ_{L2A} [-]	$1.30 \cdot 10^{-3}$	$1.30 \cdot 10^{-3}$	0.03	$9.00 \cdot 10^{-4}$	$9.00 \cdot 10^{-4}$	−4.84

is evaluated before and after temperature effect compensation. The standard deviation of the *k-th* feature (e.g., LVDT_2) was computed in two different ways. First, the overall standard deviation is computed for the entire period (*complete*) available (one year for the training set, three months for the test set). Secondly, the standard deviation is extracted every week, and then the mean value is computed across all the weeks (*week*). The table shows a sensible higher reduction in standard deviations considering the *complete* period rather than the one computed weekly, which means that the static linear regression is more effective on the seasonal component rather than the daily thermal effects. A possible explanation for this can be that most of the temperature-feature relations are non-linear in their higher frequency behaviour.

The reduction in standard deviation following temperature compensation can vary significantly, ranging from a few percentage points to over 90%. This reduction largely depends on the correlation between each feature and the temperatures before compensation. It can be demonstrated that Eq. (10) holds between the ratio of the residual standard deviation over the total standard deviation and the multiple correlation coefficient R, which is the natural extension of the linear correlation coefficient in case of more regressors(Abdi, 2007):

$$\frac{s_R}{s_Y} = \sqrt{1 - R^2} \tag{10}$$

s_R represents standard deviation of the residual signal obtained by linear regression, whereas S_Y identifies the standard deviation of the raw signals before linear regression is applied. Furthermore, R is the square root of the coefficient of determination, commonly denoted as R^2. Eq. (10) means that all the regression points should lie on a semicircle in a $\frac{s_R}{s_Y} - R$ plane.

This is confirmed in Fig. 11(a), where the reduction in standard deviation achieved during the training period is plotted against the modulus of the multiple correlation coefficient, given the symmetry of the problem. Fig. 11(b) shows the same data points obtained for the test set. Although there is an overall reduction in performance, most of the features remain close to the semicircle, indicating consistent results. By observing the feature types of the data points, it is clear that static linear regression is more effective on some features than others; this is the case for LVDTs and strain gauges, whereas the correlation between dampings and temperatures appears generally weak. The reduction achieved with linear regression is practically negligible for a correlation coefficient below 0.4–0.5, which suggests that other models than linear should be used in that case. Finally, Fig. 12 presents a quantitative comparison of the purged standard deviation between the training and test datasets.

In this figure, unitary values represent ideal conditions, demonstrating that the residual variability after compensating for thermal effects is independent of the observed period's length and, more importantly,

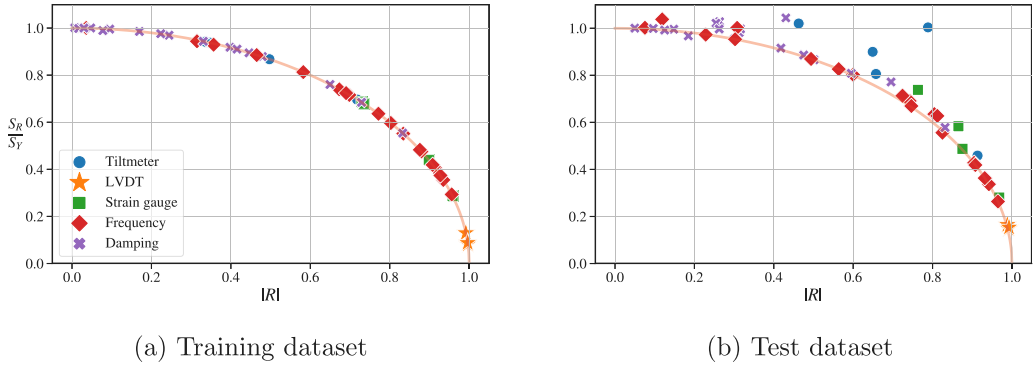

Fig. 11. Relationship between multiple correlation coefficient with temperature and remaining standard deviation, post thermal compensation, across all analysed features.

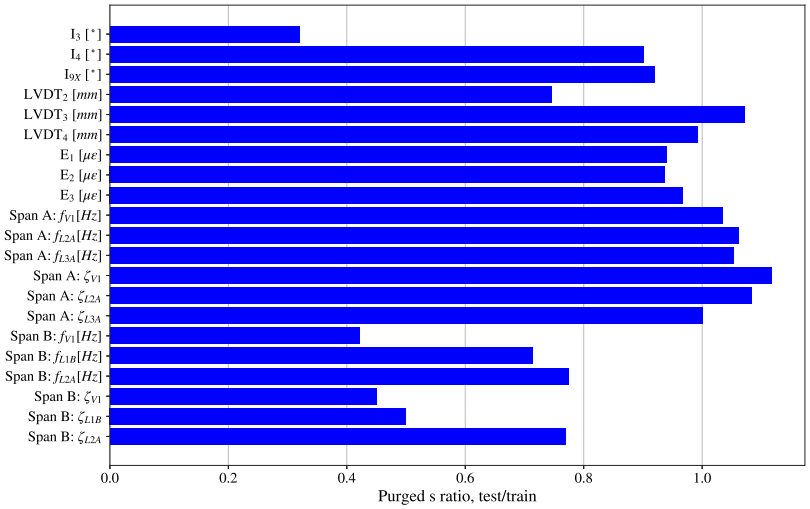

Fig. 12. Standard deviation ratio between test and training datasets, after temperature compensation, for features listed in Table 3.

that the multiple linear regression evaluated in training performs well even in fitting the test dataset. Thus, values lower than one are associated with a decline in multiple linear regression performance in the test compared to training. Conversely, values greater than one are likely correlated with lower intrinsic variability of the test dataset due to its shorter temporal extent (i.e. test dataset exhibits a lower s_y due to its reduced length, yet maintains a comparable s_R). To further reduce the variability of the signals, moving averages with different time windows are applied to the residuals (second phase of the two-step EOVs treatment), and the resulting standard deviations are used to compute the MDA curves. In Fig. 13, as examples, the MDA curves for sensor I_6 and span A natural frequency *L3A* are shown. The effect of the moving averages in shrinking the distributions is immediately visible.

Two main outputs can be generally inferred from observing the minimum detectable anomaly curves:

- If an estimation of the effect of damage on a feature is available (i.e. by simulating a damage with a finite element method analysis), MDA curves provide a way to estimate how long it is required to wait until the anomaly can be observed with a sufficient confidence level. The effect of damage in a feature can be represented as a horizontal line in Fig. 13, which intersects every MDA curve one single time.
- MDA curves allow the creation of control charts for monitoring purposes. A feature signal, averaged with a proper time window, can be compared with the MDA values for the same time window allowing the monitoring of the bridge behaviour on a *windowing* basis.

An example of the latter is shown in Fig. 14 and Fig. 15, where the residuals of sensors $LVDT_3$ (please refer to Fig. 2) and natural frequency L3 A (referred to span A) are averaged daily (a) and monthly (b). Under the hypothesis that the residuals distribution is Gaussian, in case a double confidence interval is addressed, 95% of the values should fall between the two orange dashed lines. If this does not happen, the system is encountering a statistical anomaly. The advantage of using moving averages is that, based on the window length which raised the anomaly, one might deduce the velocity evolution of the anomalous behaviour.

5. Conclusions

This work focuses on the continuous monitoring of a double-span Warren truss bridge, currently in service on a regional Italian railway line. The setup of the monitoring system is first proposed, with a focus on sensor placement and acquisition logic. Regarding data analysis, the authors presented:

- An automated operational modal analysis (AOMA) approach based on the covariance-driven stochastic subspace identification (SSI-COV) algorithm for continuous identification of bridge modal parameters.
- A two-step approach aimed at reducing environmental variability through linear regression and residual variability through a

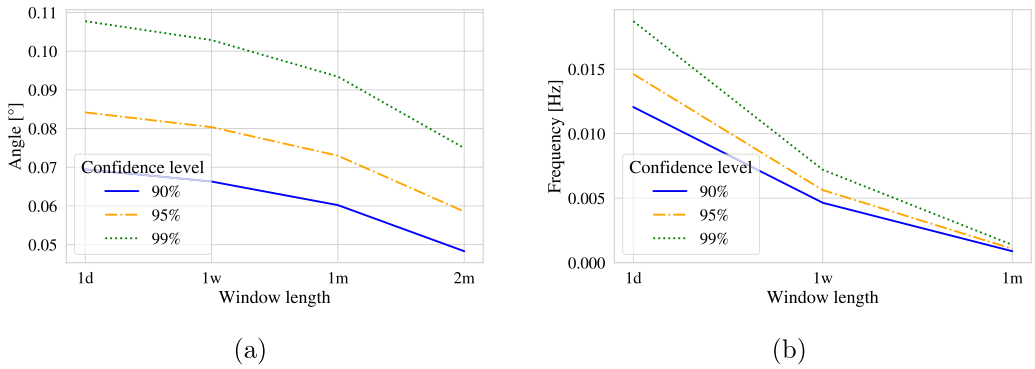

Fig. 13. Minimum detectable anomaly (MDA) curves for tiltmeter I_6 (a) and span A frequency L3 A (b). Please notice that 1d and 1w refers to a one-day and a one-week windowing interval respectively. Moreover, 1 m and 2 m identifies 1-month-long and 2-month-long intervals.

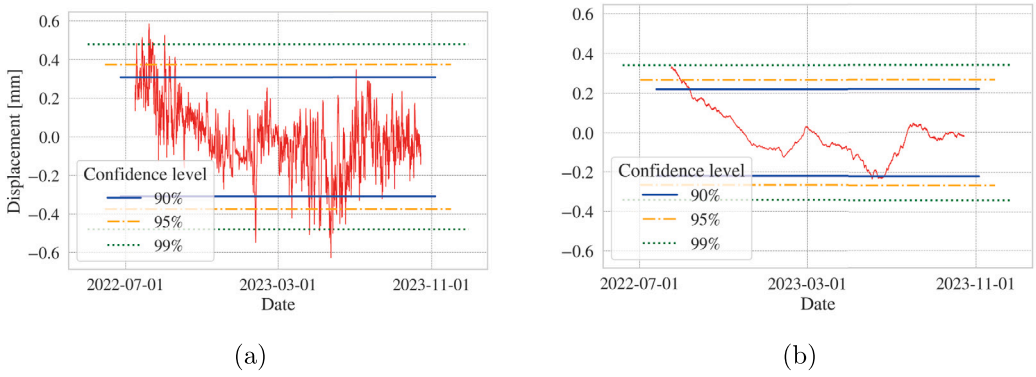

Fig. 14. Behaviour of sensor $LVDT_3$ for daily moving average (a) and monthly moving average (b) and corresponding MDA values (horizontal lines).

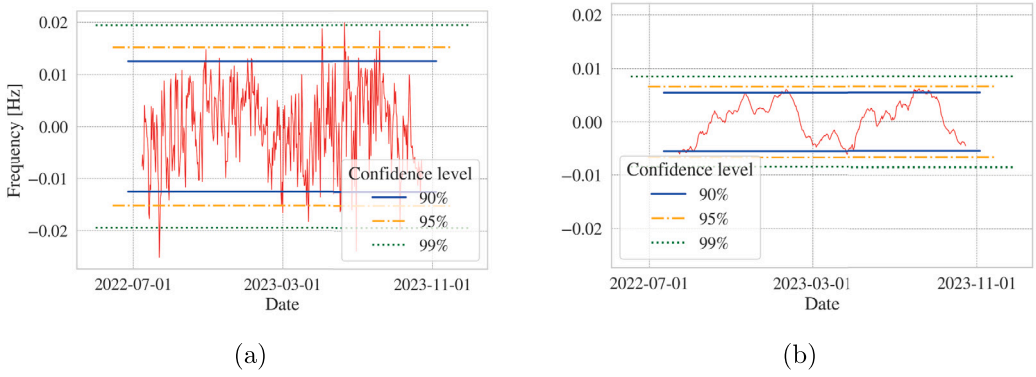

Fig. 15. Behaviour for span A natural frequency L3 A with no moving average (a) and monthly moving average (b) and corresponding MDA values (horizontal lines).

moving average operation, in order to assess anomaly evolution. This method is potentially capable of rapidly detecting intense, fast-evolving damages, while also identifying minimal intensity damages that evolve slowly by filtering out variability unrelated to the damage itself through moving averages with longer windows.

The presented permanent SHM system, installed on a railway truss bridge, which is common in northern Italy, is capable of automatically synthesizing information from large amounts of acquired data. The work led to the following main conclusions:

1. Bridge responses (measured through tiltmeters, strain gauges, and LVDTs) and natural frequencies were found to be highly dependent on temperature, in agreement with past studies. Conversely, damping ratios showed mixed behaviour, and MAC was found to be insensitive to temperature variations, confirming previous literature.
2. The treatment of the EOVs was carried out using a combination of multiple linear regression and moving averages to further reduce signal variability. Compared to other studies, this approach addresses the dynamic evolution of signals over time, making it possible to distinguish between potential underlying damages based on their evolution dynamics. Considering the importance of interpretability in SHM problems, the ability to distinguish between different scenarios is crucial for assisting decision-makers.
3. The paper explores the minimum detectable anomaly (MDA) curves, which serve a dual purpose: first, to establish how long

it will be necessary to wait before an anomaly of a certain intensity can be observed, and second, to create control charts, as demonstrated in this work.

The results presented are encouraging, but several limitations are evident. The two-step procedure for data normalization is effective in reducing signal variability. However, the resulting signals should be combined with the outcomes of other analyses to transform the measurements into comprehensive information. For example, a finite element model of the bridge could aid in understanding the actual structure configuration based on the behaviour of the purged signals. Future work must investigate how to effectively exploit the output of the proposed analysis to automatically detect potential anomalies onsets.

CRediT authorship contribution statement

Antonio Argentino: Writing – review & editing, Writing – original draft, Visualization, Methodology, Investigation, Data curation, Conceptualization. **Luca Radicioni:** Writing – review & editing, Writing – original draft, Visualization, Software, Methodology, Investigation, Data curation, Conceptualization. **Francesco Morgan Bono:** Writing – review & editing, Writing – original draft, Software, Methodology, Data curation. **Lorenzo Bernardini:** Writing – review & editing, Writing – original draft, Data curation, Conceptualization. **Lorenzo Benedetti:** Writing – review & editing, Writing – original draft, Supervision. **Gabriele Cazzulani:** Writing – review & editing, Supervision, Conceptualization. **Claudio Somaschini:** Writing – review & editing, Supervision, Conceptualization. **Marco Belloli:** Supervision, Project administration.

Declaration of competing interest

The authors declare that they have no known competing financial interests or personal relationships that could have appeared to influence the work reported in this paper.

References

Abdi, H., 2007. Multiple correlation coefficient. Encycl. Meas. Stat. 648 (651), 19.

Aflatooni, M., Chan, T.H., Thambiratnam, D.P., 2014. Synthetic rating procedures for railway bridges. J. Bridg. Eng. 19 (12), http://dx.doi.org/10.1061/(ASCE)BE.1943-5592.0000623.

Argentino, A., Bernardini, L., Benedetti, L., Cazzulani, G., Somaschini, C., Belloli, M., 2023. An automated algorithm for experimental OMA: Application on a warren truss railway bridge with a permanent monitoring system. In: Proceedings of International Conference on Experimental Vibration Analysis for Civil Engineering Structures. Milan, Italy, pp. 50–60. http://dx.doi.org/10.1007/978-3-031-39109-5_6.

Benedetti, L., Bono, F.M., Radicioni, L., Belloli, M., 2023. Design and application of a statistical learning methodology to remove temperature effect on static signals for bridge structural health monitoring. Struct. Heal. Monit. 2023, http://dx.doi.org/10.12783/shm2023/36794.

Bono, F.M., Radicioni, L., Cinquemani, S., Benedetti, L., Cazzulani, G., Somaschini, C., Belloli, M., 2023. A deep learning approach to detect failures in bridges based on the coherence of signals. Futur. Internet 15 (4), 119. http://dx.doi.org/10.3390/fi15040119.

Borlenghi, P., Gentile, C., D'Angelo, M., Ballio, F., 2024. Long-term monitoring of a masonry arch bridge to evaluate scour effects. Constr. Build. Mater. 411, 134580. http://dx.doi.org/10.1016/j.conbuildmat.2023.134580.

Brunton, S.L., Kutz, J.N., 2019. Data-Driven Science and Engineering: Machine Learning, Dynamical Systems, and Control. Cambridge University Press, http://dx.doi.org/10.1017/9781009089517.

Caspani, V.F., Tonelli, D., Poli, F., Zonta, D., 2022. Designing a structural health monitoring system accounting for temperature compensation. Infrastructures 7 (1), 5. http://dx.doi.org/10.3390/infrastructures7010005.

Civera, M., Sibille, L., Zanotti Fragonara, L., Ceravolo, R., 2023. A DBSCAN-based automated operational modal analysis algorithm for bridge monitoring. Measurement 208, 112451. http://dx.doi.org/10.1016/j.measurement.2023.112451.

Comanducci, G., Magalhães, F., Ubertini, F., Cunha, Á., 2016. On vibration-based damage detection by multivariate statistical techniques: Application to a long-span arch bridge. Struct. Heal. Monit. 15 (5), 505–524. http://dx.doi.org/10.1177/1475921716650630.

Cross, E., Koo, K., Brownjohn, J., Worden, K., 2013. Long-term monitoring and data analysis of the Tamar Bridge. Mech. Syst. Signal Process. 35 (1), 16–34. http://dx.doi.org/10.1016/j.ymssp.2012.08.026.

Deraemaeker, A., Worden, K., 2012. New Trends in Vibration Based Structural Health Monitoring. Springer Science & Business Media, http://dx.doi.org/10.1007/978-3-7091-0399-9.

Dinas, A., Nikolaidis, T., Baniotopoulos, C., 2017. Sustainable restoration criteria for a historical steel railway bridge. Procedia Environ. Sci. 38, 578–585. http://dx.doi.org/10.1016/j.proenv.2017.03.131.

Ewins, D.J., 2009. Modal Testing: Theory, Practice and Application. John Wiley & Sons.

Figueiredo, E., Radu, L., Worden, K., Farrar, C.R., 2014. A Bayesian approach based on a Markov-chain Monte Carlo method for damage detection under unknown sources of variability. Eng. Struct. 80, 1–10. http://dx.doi.org/10.1016/j.engstruct.2014.08.042.

Gianesini, B.M., Cortez, N.E., Antunes, R.A., Vieira Filho, J., 2021. Method for removing temperature effect in impedance-based structural health monitoring systems using polynomial regression. Struct. Heal. Monit. 20 (1), 202–218. http://dx.doi.org/10.1177/1475921720917126.

Giordano, P.F., Limongelli, M.P., 2022. The value of structural health monitoring in seismic emergency management of bridges. Struct. Infrastruct. Eng. 18 (4), 537–553. http://dx.doi.org/10.1080/15732479.2020.1862251.

Giordano, P.F., Turksezer, Z., Previtali, M., Limongelli, M.P., 2022. Damage detection on a historic iron bridge using satellite DInSAR data. Struct. Heal. Monit. 21 (5), 2291–2311. http://dx.doi.org/10.1177/14759217211054350.

Gordan, M., Sabbagh-Yazdi, S.-R., Ismail, Z., Ghaedi, K., Carroll, P., McCrum, D., Samali, B., 2022. State-of-the-art review on advancements of data mining in structural health monitoring. Measurement 193, 110939. http://dx.doi.org/10.1016/j.measurement.2022.110939.

Han, Q., Ma, Q., Xu, J., Liu, M., 2021. Structural health monitoring research under varying temperature condition: A review. J. Civ. Struct. Heal. Monit. 11, 149–173. http://dx.doi.org/10.1007/s13349-020-00444-x.

Iacovino, C., Turksezer, Z.I., Giordano, P.F., Limongelli, M.P., 2022. Comparison of bridge inspection policies in terms of data quality. J. Bridg. Eng. 27 (3), http://dx.doi.org/10.1061/(ASCE)BE.1943-5592.0001831.

Jiang, W.J., Kim, C.W., Goi, Y., Zhang, F.L., 2022. Data normalization and anomaly detection in a steel plate-girder bridge using LSTM. ASCE-ASME J. Risk Uncertain. Eng. Syst., Part A: Civ. Eng. 8 (1), 04021082. http://dx.doi.org/10.1061/AJRUA6.0001203.

Keshmiry, A., Hassani, S., Mousavi, M., Dackermann, U., 2023. Effects of environmental and operational conditions on structural health monitoring and non-destructive testing: A systematic review. Buildings 13 (4), 918. http://dx.doi.org/10.3390/buildings13040918.

Khoa, N.L., Zhang, B., Wang, Y., Chen, F., Mustapha, S., 2014. Robust dimensionality reduction and damage detection approaches in structural health monitoring. Struct. Heal. Monit. 13 (4), 406–417. http://dx.doi.org/10.1016/j.engstruct.2025.119957.

Kvåle, K.A., Øiseth, O., Rønnquist, A., 2017. Operational modal analysis of an end-supported pontoon bridge. Eng. Struct. 148, 410–423. http://dx.doi.org/10.1016/j.engstruct.2017.06.069.

Langone, R., Reynders, E., Mehrkanoon, S., Suykens, J.A., 2017. Automated structural health monitoring based on adaptive kernel spectral clustering. Mech. Syst. Signal Process. 90, 64–78. http://dx.doi.org/10.1016/j.ymssp.2016.12.002.

Limongelli, M., 2019. Vibration-based structural health monitoring: Challenges and opportunities. In: Proceedings of Advances in Engineering Materials, Structures and Systems: Innovations, Mechanics and Applications-Proceedings of the 7th International Conference on Structural Engineering, Mechanics and Computation, 2019. CRC Press/Balkema, pp. 1999–2004. http://dx.doi.org/10.1201/9780429426506-344.

Limongelli, M.P., Gentile, C., Biondini, F., di Prisco, M., Ballio, F., Zonno, G., Borlenghi, P., Bianchi, S., Capacci, L., Anghileri, M., Zani, G., Scalbi, A., Flores Ferreira, K., D'Angelo, M., Cazzulani, G., Benedetti, L., Somaschini, C., Bernardini, L., Belloli, M., Resta, F., Vigo, P., Colombo, A., 2022. Bridge structural monitoring: the Lombardia regional guidelines. Struct. Infrastruct. Eng. 20 (4), 461–484. http://dx.doi.org/10.1080/15732479.2022.2107023.

Lin, W., Yoda, T., Taniguchi, N., 2014. Rehabilitation and restoration of old steel railway bridges: Laboratory experiment and field test. J. Bridg. Eng. 19 (5), http://dx.doi.org/10.1061/(ASCE)BE.1943-5592.0000574.

Magalhães, F., Cunha, A., Caetano, E., 2009. Online automatic identification of the modal parameters of a long span arch bridge. Mech. Syst. Signal Process. 23 (2), 316–329. http://dx.doi.org/10.1016/j.ymssp.2008.05.003.

Magalhães, F., Cunha, Á., Caetano, E., 2012. Vibration based structural health monitoring of an arch bridge: From automated OMA to damage detection. Mech. Syst. Signal Process. 28, 212–228. http://dx.doi.org/10.1016/j.ymssp.2011.06.011.

Mariani, S., Kalantari, A., Kromanis, R., Marzani, A., 2024. Data-driven modeling of long temperature time-series to capture the thermal behavior of bridges for SHM purposes. Mech. Syst. Signal Process. 206, 110934. http://dx.doi.org/10.1016/j.ymssp.2023.110934.

Mousavi, M., Gandomi, A.H., 2021. Structural health monitoring under environmental and operational variations using MCD prediction error. J. Sound Vib. 512, 116370. http://dx.doi.org/10.1016/j.jsv.2021.116370.

Nassar, M., Amleh, L., 2023. The effect of projected air temperatures on concrete box girders thermal gradients and effective temperatures in Canada. Results Eng. 20, 101453. http://dx.doi.org/10.1016/j.rineng.2023.101453.

Orcesi, A.D., Frangopol, D.M., 2011. Optimization of bridge maintenance strategies based on structural health monitoring information. Struct. Saf. 33 (1), 26–41. http://dx.doi.org/10.1016/j.strusafe.2010.05.002.

Pastor, M., Binda, M., Harčarik, T., 2012. Modal assurance criterion. Procedia Eng. 48, 543–548. http://dx.doi.org/10.1016/j.proeng.2012.09.551.

Radicioni, L., Bernardini, L., Bono, F.M., Anghileri, M., Capacci, L., Cazzulani, G., Somaschini, C., Pande, A.K., Biondini, F., Cinquemani, S., et al., 2023. Structural health monitoring of a steel truss railway bridge studying its low frequency response. Ce/Papers 6 (5), 876–885. http://dx.doi.org/10.1002/cepa.2184.

Reynders, E., Wursten, G., Roeck, G.D., 2014. Output-only structural health monitoring in changing environmental conditions by means of nonlinear system identification. Struct. Heal. Monit. 13 (1), 82–93. http://dx.doi.org/10.1177/1475921713502836.

Salehi, M., Erduran, E., 2022. Identification of boundary conditions of railway bridges using artificial neural networks. J. Civ. Struct. Heal. Monit. 12 (5), 1223–1246. http://dx.doi.org/10.1007/s13349-022-00613-0.

Tomassini, E., García-Macías, E., Reynders, E., Ubertini, F., 2023. Model-assisted clustering for automated operational modal analysis of partially continuous multi-span bridges. Mech. Syst. Signal Process. 200, 110587. http://dx.doi.org/10.1016/j.ymssp.2023.110587.

Uyanık, G.K., Güler, N., 2013. A study on multiple linear regression analysis. Procedia-Social Behav. Sci. 106, 234–240. http://dx.doi.org/10.1016/j.sbspro.2013.12.027.

Vardanega, P., Webb, G., Fidler, P., Huseynov, F., Kariyawasam, K., Middleton, C., 2022. 32 - bridge monitoring. In: Pipinato, A. (Ed.), Innovative Bridge Design Handbook (Second Edition), second ed. Butterworth-Heinemann, pp. 893–932. http://dx.doi.org/10.1016/B978-0-12-823550-8.00023-8.

Wang, Z., Yang, D.H., Yi, T.H., Zhang, G.H., Han, J.G., 2022. Eliminating environmental and operational effects on structural modal frequency: A comprehensive review. Struct. Control. Heal. Monit. 29 (11), e3073. http://dx.doi.org/10.1002/stc.3073.

Xia, Y., Chen, B., Weng, S., Ni, Y.Q., Xu, Y.L., 2012. Temperature effect on vibration properties of civil structures: a literature review and case studies. J. Civ. Struct. Heal. Monit. 2, 29–46. http://dx.doi.org/10.1007/s13349-011-0015-7.

Zhou, G.D., Yi, T.H., 2014. A summary review of correlations between temperatures and vibration properties of long-span bridges. Math. Probl. Eng. 2014, http://dx.doi.org/10.1155/2014/638209.

Zini, G., Betti, M., Bartoli, G., 2022. A quality-based automated procedure for operational modal analysis. Mech. Syst. Signal Process. 164, 108173. http://dx.doi.org/10.1016/j.ymssp.2021.108173.